



Cite this: *Lab Chip*, 2023, 23, 4540

Enhanced cardiomyocyte structural and functional anisotropy through synergetic combination of topographical, conductive, and mechanical stimulation†

Jongyun Kim,^{ad} Arunkumar Shanmugasundaram,^{ad} Cheong Bin Lee,^a Jae Rim Kim,^a Jeong Jae Park,^a Eung-Sam Kim,^{ib bc} Bong-Kee Lee^{ib ac} and Dong-Weon Lee^{ib *acd}

Drug-induced cardiotoxicity, a significant concern in the pharmaceutical industry, often results in the withdrawal of drugs from the market. The main cause of drug-induced cardiotoxicity is the use of immature cardiomyocytes during *in vitro* drug screening procedures. Over time, several methods such as topographical, conductive, and mechanical stimulation have been proposed to enhance both maturation and contractile properties of these cardiomyocytes. However, the synergistic effects of integrating topographical, conductive, and mechanical stimulation for cardiomyocyte maturation remain underexplored and poorly understood. To address this limitation, herein, we propose a grooved polydimethylsiloxane (PDMS) membrane embedded with silver nanowires (AgNWs-E-PDMS). The proposed AgNWs-E-PDMS membrane enhances the maturation of cardiomyocytes and provides a more accurate evaluation of drug-induced cardiotoxicity. When subjected to 10% tensile stress on the AgNWs-E-PDMS membrane, cardiomyocytes displayed substantial enhancements. Specifically, the contraction force, sarcomere length, and connexin-43 (Cx43) expression are increased by 2.0-, 1.5-, and 2.4-times, respectively, compared to the control state. The practical feasibility of the proposed device as a drug screening platform is demonstrated by assessing the adverse effects of lidocaine on cardiomyocytes. The contraction force and beat rate of lidocaine treated cardiomyocytes cultured on the AgNWs-E-PDMS membrane under mechanical stimulation decreased to 0.9 and 0.64 times their initial values respectively, compared to 0.6 and 0.51 times in the control state. These less pronounced changes in the contraction force and beat rate signify the superior drug response in the cardiomyocytes, a result of their enhanced maturation and growth on the AgNWs-E-PDMS membrane combined with mechanical stimulation.

Received 24th May 2023,
Accepted 17th September 2023

DOI: 10.1039/d3lc00451a

rsc.li/loc

Introduction

Cardiovascular diseases, such as heart attacks and strokes, are responsible for a significant number of deaths worldwide.^{1–3} As a result, extensive research efforts have been devoted to developing drugs for targeting the specific mechanism involved in the development and progression of

these diseases. Despite significant progress in cardiovascular drug development, several drugs have been withdrawn from the market due to drug induced cardiotoxicity.^{4,5} The main cause of drug induced cardiotoxicity is the use of immature cardiomyocytes in *in vitro* drug screening procedures. The immature cardiomyocytes used in *in vitro* drug screening applications do not exactly replicate *in vivo* physiological conditions.^{6,7} Therefore, the development of more accurate *in vitro* screening platforms that can enhance the maturation of cultured cardiomyocytes and enable the screening of drug-induced cardiotoxicity is highly desired.

Over the years, numerous strategies have been proposed to promote the maturation of cardiomyocytes, including mechanical stimulation, topographical stimulation, and the implementation of conductive materials as cell culture substrates. Mechanical stimulation, an effective approach designed to mimic *in vivo* microenvironments, facilitates the

^a MEMS and Nanotechnology Laboratory, School of Mechanical Engineering, Chonnam National University, Gwangju 61186, Republic of Korea. E-mail: mems@jnu.ac.kr

^b Department of Biological Sciences, Chonnam National University, Gwangju, 61186, Republic of Korea

^c Center for Next-Generation Sensor Research and Development, Chonnam National University, Gwangju 61186, Republic of Korea

^d Advanced Medical Device Research Center for Cardiovascular Disease, Chonnam National University, Gwangju 61186, Republic of Korea

† Electronic supplementary information (ESI) available. See DOI: <https://doi.org/10.1039/d3lc00451a>

structural and functional maturation of cardiomyocytes.^{8–16} For instance, a study by Nitsan *et al.* examined the mechanical communication between adjacent cells, revealing that a cell can interact mechanically with its neighbouring cells through deformation on the cell culture substrate. Their research further demonstrated that signals originating from proximate microenvironments could drastically improve the maturation profile of cardiomyocytes.¹⁰ Tang *et al.*, in a similar manner, provided evidence that adjacent cells could influence each other through mechanical stimulation, leading to synchronized cell contraction over extended periods and subsequently promoting cardiomyocyte maturation.¹⁷ Mechanical stimulation has the capability to align cardiomyocytes along the stretch axis, mimicking the anisotropic orientation found in native heart tissue. However, this technique does not guarantee absolute precision in the alignment direction of cardiomyocytes, owing to divergency in the cellular responses to mechanical cues.

The simultaneous application of topographical and mechanical stimulation has emerged as a potent strategy to enhance the precision of cardiomyocyte alignment in the desired direction. Under the combined influence of topographical and mechanical stimulation, cardiomyocytes exhibit a significant upregulation in gene expression compared to those subjected to each stimulation independently. Topographical stimulation facilitates cardiomyocyte alignment along the groove direction, effectively simulating the native cardiac tissue microenvironment, and thereby fostering cellular organization and maturation. For instance, Dou *et al.* studied the impact of mechanical stimulation on the cytoskeletal organization and structural development of cardiomyocytes.¹⁸ Furthermore, Jeong *et al.* utilized a circular diaphragm featuring nano-groove patterns to mechanically stimulate cardiomyocytes, with the aim of assessing structural enhancements in cardiomyocytes subjected to 6% mechanical stress.¹⁹ Similarly, Siddique *et al.* demonstrated that the co-application of mechanical and topographical stimulation could increase the sarcomere length in cultured cardiomyocytes to approximately $1.97 \pm 0.03 \mu\text{m}$ and upregulate Cx43 expression to around 1.57, compared with a sarcomere length of approximately $1.82 \pm 0.02 \mu\text{m}$ and a Cx43 expression level of about 1.32 in the absence of topographical stimulation.²⁰ These studies emphasize the potential of such integrative cell culture platforms for enhancing the maturation of cardiomyocytes effectively. However, cyclic mechanical stimulation applied to a circular diaphragm can generate strain fluctuations across the diaphragm, leading to variable stretch intensities within the substrate. Furthermore, the impact of conductive substrates on cardiomyocyte maturation has not been investigated in these studies.

Conductive materials such as conductive polymers,^{21–23} carbon-based materials,^{24,25} gold,²⁶ and silver²⁷ have been extensively employed as cell culture platforms with the aim of enhancing the maturation process of cardiomyocytes. Among several conductive materials, AgNWs have received considerable attention due to their superior electrical conductivity and exceptional mechanical flexibility.^{28–34}

Nonetheless, the practical application of AgNWs is impeded by their high susceptibility to oxidation upon exposure to air, which could potentially induce adverse cytotoxic effects in cultured cardiomyocytes.³⁵ To overcome this limitation, several protective layers have been proposed to enhance the stability, and thereby the viability, of AgNWs.^{36–40} Encapsulation of AgNWs within a PDMS matrix represents a promising approach, the potential utility of which has been demonstrated in various applications. Despite this progress, the experimental validation of AgNWs encapsulated within PDMS, both as a cell culture substrate in conjunction with topographical and mechanical stimulation and as a drug screening platform for the evaluation of cardiotoxicity, has yet to be firmly established.

Herein, we propose a grooved PDMS membrane embedded with AgNWs as a cell culture platform, engineered to be coupled with mechanical stimulation, aiming to facilitate cardiomyocyte maturation and to evaluate drug-induced cardiotoxicity. The incorporation of AgNWs within the PDMS membrane establishes an electrically conductive microenvironment that improves intercellular communication and electrical coupling, thus enhancing the maturation of cultured cardiomyocytes. Furthermore, the platform's unique ability to provide simultaneous topographical and mechanical stimulation effectively simulates the biophysical and electrical cues found in native tissues, thereby further promoting cardiomyocyte maturation. Neonatal rat ventricular myocytes (NRVMs) were isolated and seeded on the proposed device, and then subjected to 10% applied tensile stress at a frequency of 1 Hz. Maturation progress in the cardiomyocytes was evaluated through immunocytochemical analysis. Our results revealed a significant enhancement in sarcomere length and Cx43 expression within cardiomyocytes cultivated on the AgNWs–E-PDMS membrane under the influence of combined mechanical and topographical stimulation, compared to the control state. To further validate the functional utility of this platform, we deployed it as a drug screening tool to investigate the cytotoxic effects of lidocaine on cardiomyocytes. This work emphasizes the potential of our AgNWs–E-PDMS based platform as a versatile tool in cardiac tissue engineering and drug screening applications.

Materials and methods

Device concept, fabrication, and working mechanism

The conceptual design and working mechanism of the proposed device are illustrated schematically in Fig. 1. The system comprises functional well plates, a linear stage, a stepper motor, a moving plate integrated with a laser displacement sensor, a stage-top incubator, and a transparent acrylic case (Fig. 1a). The top and front views of the mechanical stimulation system are shown in Fig. S1.† The PDMS well plate was fabricated by curing PDMS in a 10 : 1 base-to-curing agent ratio within a polytetrafluoroethylene (PTFE) mold. The functional well plate consists of a moving

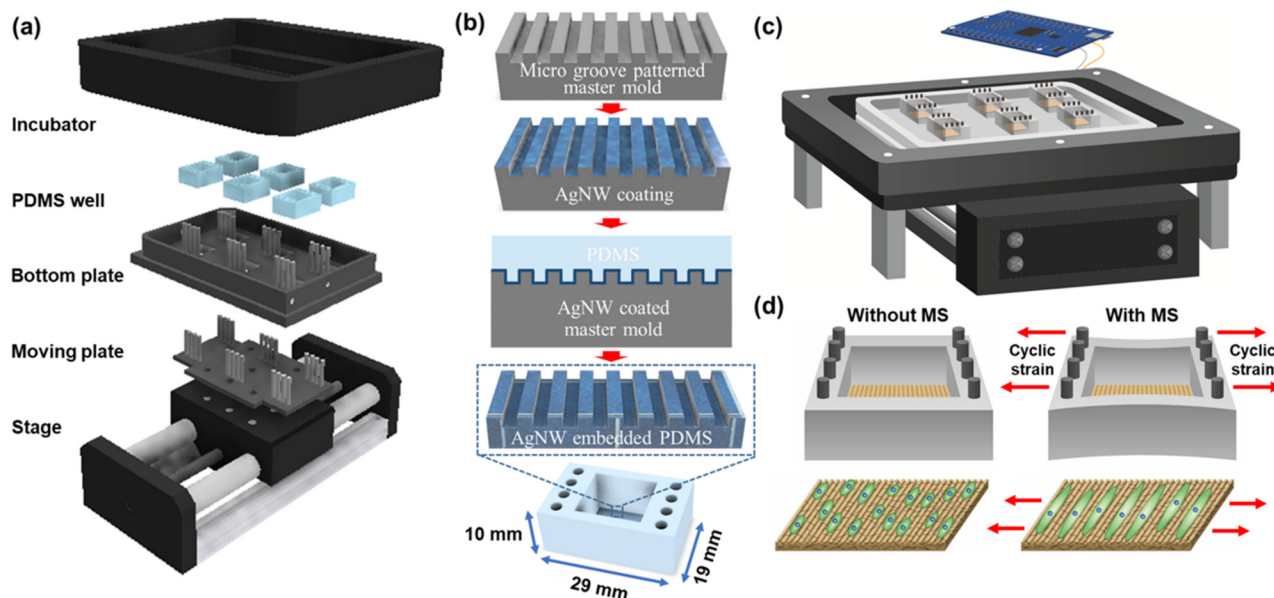


Fig. 1 (a–d) Schematic illustrating the device concept, fabrication of the groove patterned PDMS membrane and working mechanism of the proposed mechanical stimulation system.

plate equipped with a laser displacement sensor, a bottom plate, and a PDMS cell culture platform (Fig. S2†). The moving bottom plates were fabricated from anodized aluminum to withstand autoclave sterilization. The bottom plates were interconnected with a screw-type jig, facilitating the easy detachment and attachment of the PDMS well plate. To monitor the stretchability of the PDMS membrane induced by the linear motor with precision, laser displacement sensors were patterned on the moving plate. Displacement was then assessed using a laser vibrometer, which provides nanoscale accuracy. The lateral stretching of the cell culture platform was driven by a stepper motor. 3 μm groove patterns were patterned on the PDMS membrane to facilitate the topographical stimulation of the cultured cardiomyocytes. The topographical stimulation aligns the cardiomyocytes in the groove direction and promotes their maturation. AgNWs were embedded within the grooved PDMS membrane to enhance cell–cell interactions and improve the growth and maturation of the cardiomyocytes. An integrated stage-top incubator (Life Science Instrument, LCI CU-501) was used to maintain optimal environmental conditions—such as temperature, humidity, and CO_2 concentration—throughout the cell culture process. Additionally, the transparent acrylic case in the system facilitated the real-time observation of cell growth, maturation, and contractility *via* a confocal microscope.

Cell culture substrates based on groove-patterned PDMS, AgNWs surface-coated PDMS (AgNWs–S-PDMS) and AgNWs–E-PDMS, were fabricated using the following process. Firstly, a 3 μm grooved SU-8 2002 master mold was fabricated using a modified photolithography technique. In a typical fabrication process, a calculated amount of SU-8 2002 was spin-coated onto a silicon wafer at 3000 rpm for 40 s. The

SU-8 was then subjected to a soft bake at 95 $^{\circ}\text{C}$ for 1 min on a preheated hot plate. Subsequently, the SU-8 was exposed to ultraviolet light (80 mJ cm^{-2}) through a mask for 7 s, to produce a groove pattern with a width of 3 μm , a pitch distance of 3 μm , and a thickness of 1 μm . The mold was developed using an SU-8 developer (Sigma-Aldrich, USA) for 1 min, followed by a rinse with isopropyl alcohol (IPA, Sigma-Aldrich, USA). The fabricated SU-8 2002 master mold was used to fabricate the groove-patterned PDMS membrane with a thickness of 100 μm . In a typical fabrication process, a calculated amount PDMS was poured onto the SU-8 2002 master mold and then spin-coated at 800 rpm for 40 s. Following a curing process at 80 $^{\circ}\text{C}$ for 2 h, the groove-patterned bare PDMS membrane was gently detached from the SU-8 2002 master mold. To fabricate the AgNWs–S-PDMS membrane, a 0.2 mg mL^{-1} AgNW solution was directly spin-coated onto the 3 μm groove PDMS membrane at 500 rpm for 10 s, followed by 3000 rpm for 30 s. The AgNWs–E-PDMS membrane was fabricated using the following fabrication process. Firstly, a 0.2 mg mL^{-1} AgNW solution was spin-coated onto the 3 μm groove SU-8 master mold at 500 rpm for 10 s and then at 3000 rpm for 30 s. Next, a calculated amount of PDMS (with a base to curing agent ratio of 10:1) was spin-coated onto the AgNWs-coated 3 μm groove SU-8 master mold at 800 rpm for 40 s. Subsequently, the substrate was cured at 80 $^{\circ}\text{C}$ for 2 h on a hot plate. After the curing process, the AgNW-embedded PDMS membrane was carefully removed from the master mold (Fig. 1b).

The functional well plate containing cultured cardiomyocytes is placed on the moving plate, which is connected to the linear stage and stepper motor. The stepper motor drives the linear stage, causing lateral movement of the plate, and thus inducing uniaxial tension on the PDMS

membrane. As the PDMS membrane stretches laterally, the cardiomyocytes undergo external mechanical stimulation. The laser displacement sensor on the moving plate continuously measures the degree of lateral stretching exerted on the PDMS membrane. An Arduino program processed the data collected by the sensors and provided real-time feedback to control the movement of the stepper motor and maintain the desired level of mechanical stimulation (Movie S1†). The combination of groove patterns, conductive substrate, and lateral stretching enhances the maturation and growth of cultured cardiomyocytes, mimicking the *in vivo* mechanical environment. This stimulation results in improved cellular function and organization as shown in Fig. 1c.

Mechano-biology measurements

An inverted confocal microscope was used to capture live images and videos of cultured cardiomyocytes for mechanophysiological analysis. Custom-designed motion tracking software was utilized to assess cardiomyocyte contractility through the analysis of the beating activity of at least ten individual cardiomyocytes at specified regions. This software quantified the unique displacement exhibited by the cardiomyocytes during the contraction and relaxation stages.

The calculated average displacement was designated as the relative displacement for the cardiomyocytes, thereby enhancing the reliability of cardiomyocyte contractility measurements.

Results and discussion

Finite element method (FEM) simulation analysis was performed employing the ANSYS HFSS 2021 version R1 software, to identify the uniform stress distribution across the PDMS membrane. This process aimed to ensure the provision of consistent mechanical stimulation to the cultured cardiomyocytes. The simulation procedure encompassed a series of iterative steps: incrementally increasing the number of jigs, solving the FEM problem, checking for solution convergence, and iteratively repeating these steps until the determined level of precision was attained. Solution convergence was validated by establishing the delta S parameter at either 0.01 or 0.02 (Fig. S3†).

The dimensions of the PDMS membrane were fixed at 15 mm in length, 15 mm in width, and 100 μ m in thickness. Computational analysis was conducted, applying 10% tensile stress to the PDMS membrane, to investigate the variation in stress distribution with respect to the number of jigs, as shown in Fig. S4a–d.† The stress distributions were found to be 1.31 ± 0.015 mm, 1.39 ± 0.013 mm, and 1.41 ± 0.012 mm for 2, 3, and 4 jigs, respectively. The simulation analysis confirmed that all PDMS membranes exhibited maximum deformation at the centre and a lower level of deformation at the ends of the PDMS wall, where the jigs were located. Upon examining the stress distribution on the PDMS membrane, it was determined that the use of 4 jigs resulted in a uniform stress distribution.

Consequently, the PDMS well plate was designed with 4 jigs on each side to ensure consistent mechanical stimulation of the cultured cardiomyocytes (Fig. S4†).

The structural integrity of the groove-patterned PDMS, AgNWs–S-PDMS, and AgNWs–E-PDMS membranes was investigated through the optical microscopy and field emission scanning electron microscopy (FE-SEM) techniques. Optical microscopy examinations of these membranes corroborated the successful fabrication of uniformly distributed, microscale groove patterns on the PDMS membrane. Further, the presence of AgNWs was confirmed in the AgNWs–S-PDMS and AgNWs–E-PDMS substrates (Fig. 2a–c). Notably, AgNWs displayed a loosely tangled distribution on the AgNWs–S-PDMS substrate, whereas they appeared to be flawlessly embedded within the AgNWs–E-PDMS matrix. High-resolution FE-SEM images provided insights into the precisely crafted, well-defined edges of the groove patterns (Fig. 2d). Additionally, these images also depicted a homogeneous dispersion of AgNWs across the grooved PDMS surface, with an average diameter of 200 nm and lengths spanning several microns (Fig. 2e and f). The AgNWs coated on the PDMS membrane formed a three-dimensional (3D) interconnected conductive network structure that enabled excellent cell-to-cell interactions. The FE-SEM images of the AgNWs–E-PDMS membrane showed that the AgNWs were embedded homogeneously over the entire region of the PDMS matrix. The cross-sectional images of the fabricated PDMS membrane demonstrated that the nanotextures were almost uniform in size, with an average width of 3 μ m (Fig. 2g–i). The water contact angle (WCA) was measured to evaluate the hydrophobicity of the grooved PDMS membrane before and after surface modification with AgNWs (Fig. 2j). The WCA of the bare grooved PDMS membrane was found to be 105°, indicating that the surface was highly hydrophobic. After the surface modification with AgNWs, the WCA decreased to 100°, suggesting a slight reduction in the surface hydrophobicity. The elemental mappings of the AgNWs–S-PDMS and AgNWs–E-PDMS membranes demonstrate the uniform distribution of AgNWs on the PDMS membrane (Fig. 2h and i).

The surface oxidation of both AgNWs–S-PDMS and AgNWs–E-PDMS membranes was investigated, as shown in Fig. S5.† These membranes were subjected to oxygen plasma treatment at a power of 100 W for a duration of 5 min. Subsequent to this treatment, the morphology of the AgNWs on both the AgNWs–S-PDMS and AgNWs–E-PDMS membranes was examined using FE-SEM analysis. This analysis revealed distinct morphological changes in the AgNWs on the AgNWs–S-PDMS substrate as compared to those on the AgNWs–E-PDMS substrate. The formation of particle-like structures on the AgNWs was induced by oxidation. The presence of these particulate aggregates on the oxidized AgNWs has the potential to significantly reduce their electrical conductivity and introduce cytotoxic risks to the cardiomyocytes during the culture period. In contrast, the occurrence of such particulate aggregates was evidently lower

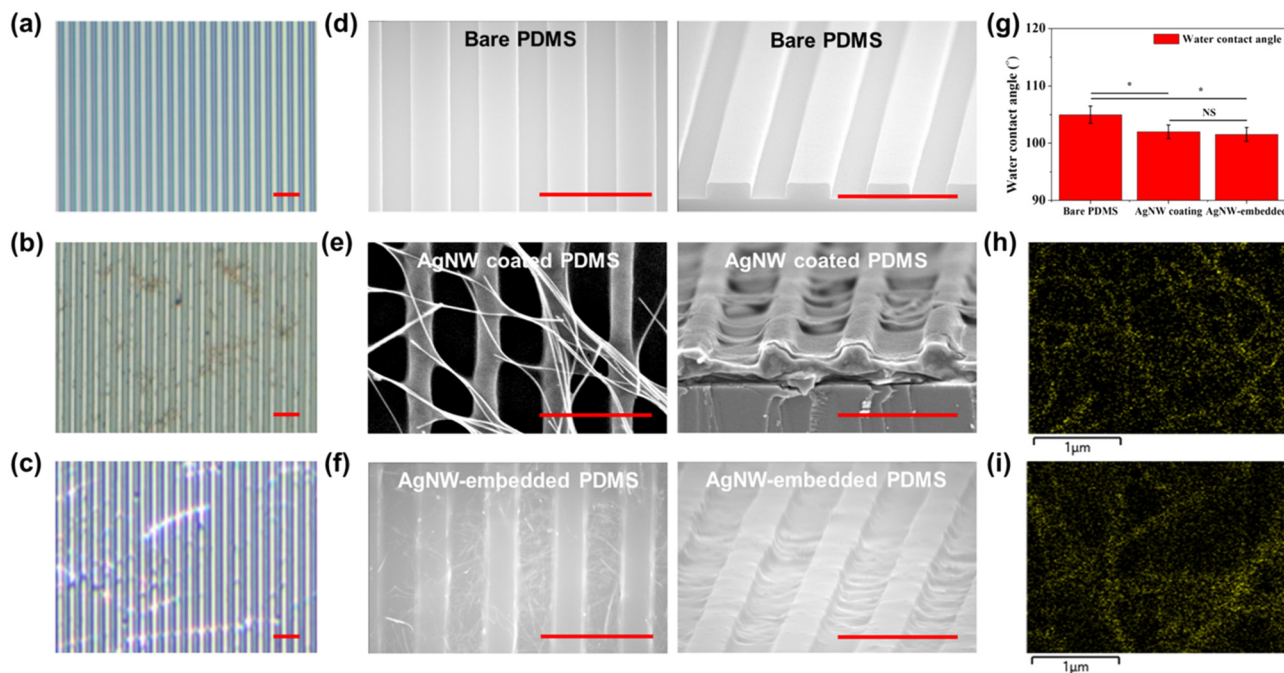


Fig. 2 Morphology and water contact angle of the as-prepared microgrooved PDMS mold. (a–c) Optical images of the as-prepared microgrooved PDMS, AgNWs–S–PDMS, and AgNWs–E–PDMS diaphragms. (d–f) Field emission scanning electron micrographs of the as-prepared microgrooved PDMS, AgNWs–S–PDMS, and AgNWs–E–PDMS diaphragms at two different magnifications. (g) Water contact angle of the bare PDMS, AgNWs–S–PDMS, and AgNWs–E–PDMS diaphragms. (h and i) Elemental mappings of the AgNWs–S–PDMS and AgNWs–E–PDMS diaphragms. Scale bar 10 μm. The bars and error bars indicate the mean \pm standard deviation ($n = 6$). NS (non-significant), $*P < 0.05$, $**P < 0.01$.

on the surface of the AgNWs–E–PDMS membrane. Notably, areas exhibiting oxidation were primarily located in areas where the AgNWs were exposed to the surface of the PDMS matrix, suggesting that the embedded PDMS layer serves as a protective layer against the oxidative degradation of the AgNWs. The integrity and durability of the AgNWs in both AgNWs–S–PDMS and AgNWs–E–PDMS membranes were assessed through a tape-peeling test. Both the membranes were affixed to a rigid substrate, and a strip of 3M adhesive tape was applied to their surfaces. A consistent force of approximately 2 N was exerted on each membrane for 3 min. Post-peeling effects on the surface topography of these substrates were then evaluated using optical microscopy and FE-SEM analyses, as shown in Fig. S6†. The AgNWs on the AgNWs–S–PDMS membrane exhibited a tendency to detach from the underlying PDMS substrate, whereas the AgNWs in the AgNWs–E–PDMS membrane demonstrated robust adhesion. In addition, we assessed the structural integrity of the AgNWs on both AgNWs–S–PDMS and AgNWs–E–PDMS membranes before and after exposure to sustained cyclic mechanical stretching at a frequency of 1 Hz for a duration of two weeks. Optical microscopy analysis was employed to evaluate the structural integrity of the AgNWs on these membranes following the mechanical stretching (Fig. S7a†). Most of the AgNWs on the surface of the AgNWs–S–PDMS membrane were detached after the two-week mechanical stretching. In contrast, the AgNWs on the AgNWs–E–PDMS membrane were largely retained, which can be attributed to the embedding structure.

To further confirm the detachment of the AgNWs, we conducted four-probe measurements to assess the surface conductivity of both AgNWs–S–PDMS and AgNWs–E–PDMS membranes (Fig. S7b†). The AgNWs–S–PDMS membrane displayed surface conductivity in the $k\Omega$ range, owing to its robust 3D interconnected conductive network. However, the sheet resistance of this membrane increased to $9.85 \pm 0.75 \text{ M}\Omega \text{ sq}^{-1}$ after two weeks of cyclic mechanical stretching, indicating significant AgNW detachment. Conversely, the initial surface conductivity of the AgNWs–E–PDMS membrane was in the range of $2.25 \pm 0.75 \text{ M}\Omega \text{ sq}^{-1}$ and remained in this range even after the stretching, highlighting the protective effect of the embedding framework.

The change in displacement of the moving plate within the mechanical stimulation system, in correlation with the number of PDMS well plates, was assessed under 10% applied tensile stress accompanied by 1 Hz mechanical stimulation (Fig. S8†). The displacement of the moving plate was monitored using a laser reflectance sensor with a laser vibrometer at nanoscale accuracy. The findings indicated that the moving plate traversed 1.77 mm in the absence of PDMS well plates, whereas the distances covered were 1.6 mm, 1.55 mm, and 1.5 mm for configurations of 2, 4, and 6 PDMS wells, respectively. Consequently, the step count required to effectuate 10% tensile stress, based on the quantity of PDMS well plates, was established as 2450 for 2 PDMS wells, 2550 for 4 PDMS wells, and 2620 for 6 PDMS wells. To apply 10% tensile stress on the cardiomyocytes cultured on the PDMS membrane with 6 PDMS well plates *in situ*, a step count of

2620 was programmed into the stepper motor. The tensile strength of both AgNWs-S-PDMS and AgNWs-E-PDMS membranes was quantitatively evaluated utilizing a Shimadzu EZ TEST-500 N tensile testing machine, as shown in Fig. S9.† Test samples were prepared with dimensions of 20 mm in length, 10 mm in width, and a thickness of 100 μm . It was observed that the tensile strength of the AgNWs-E-PDMS membrane (690 kPa) was higher than that of the AgNWs-S-PDMS membrane (630 kPa). This enhanced mechanical robustness can be attributed to the intrinsic rigidity of the AgNWs, which facilitates effective stress transfer mechanisms within the PDMS matrix.

The effect of mechanical stimulation on the proliferation and maturation of cardiomyocytes cultured on a flat PDMS membrane, both in the absence and presence of mechanical stimulation, was examined as shown in Fig. 3. Neonatal ventricular myocytes (NRVMs) were isolated from the hearts of one-day-old Sprague–Dawley rats. The detailed NRVM isolation process is described in detail in the ESI.† All animal experiments adhered to the prescribed principles of laboratory animal care and relevant national regulations, and received approval from the Animal Ethics Committee at Chonnam National University (license number: CNU IACUC-YB-2023-48).⁴¹ Cardiomyocytes cultured on the flat PDMS membrane began to demonstrate coordinated beating patterns on the third day. The cardiomyocytes cultured on a flat PDMS membrane were subjected to mechanical stimulation (applied tensile stress of 10% at a frequency of 1 Hz) from days 4 to 10.

The optical microscopy images of the cardiomyocytes revealed that those cultured on the flat PDMS membrane without mechanical stimulation displayed isotropic characteristics. In contrast, cardiomyocytes exposed to mechanical stimulation demonstrated anisotropic behavior and aligned themselves perpendicularly to the direction of

the applied mechanical stimulation (Fig. S10a†). The proliferation and maturation of cardiomyocytes were investigated through immunocytochemical (ICC) staining analysis performed on the tenth day of culture. The detailed methodology for the ICC staining analysis is provided in the ESI.† The ICC staining images of cardiomyocytes cultured on the PDMS membrane, both with and without mechanical stimulation, are shown in Fig. S10b.† The ICC staining images verified that the DAPI and α -actinin orientation of the cardiomyocytes cultured on the flat PDMS membrane with mechanical stimulation aligned perpendicularly to the direction of the mechanical stimulation. Conversely, the cardiomyocytes cultured without mechanical stimulation exhibited random alignments in various directions.

The combined effect of topographical and mechanical stimulation on the proliferation and maturation of cultured cardiomyocytes was investigated as shown in Fig. 3. The sarcomere length of cardiomyocytes cultured on a grooved PDMS membrane, in both the presence and absence of mechanical stimulation, was quantified through ICC staining analysis. The sarcomere length is one of the important factors that determine the cardiac contractile functionality since it reflects the degree of cardiomyocyte maturation and maximal contraction force. The sarcomere length is defined as the distance between two Z discs which are the fundamental units of muscular contraction. The cardiomyocytes cultured on a flat PDMS membrane without mechanical stimulation exhibited a sarcomere length of $1.71 \pm 0.01 \mu\text{m}$. In contrast, the cardiomyocytes exposed to mechanical stimulation at 10% applied tensile stress at a frequency of 1 Hz for 7 days exhibited a sarcomere length of $1.78 \pm 0.02 \mu\text{m}$. The cardiomyocytes cultured on the grooved PDMS membrane exhibited a sarcomere length of $1.81 \pm 0.02 \mu\text{m}$ without mechanical stimulation, and $1.82 \pm 0.015 \mu\text{m}$ with mechanical stimulation (Fig. 3a). The alignment

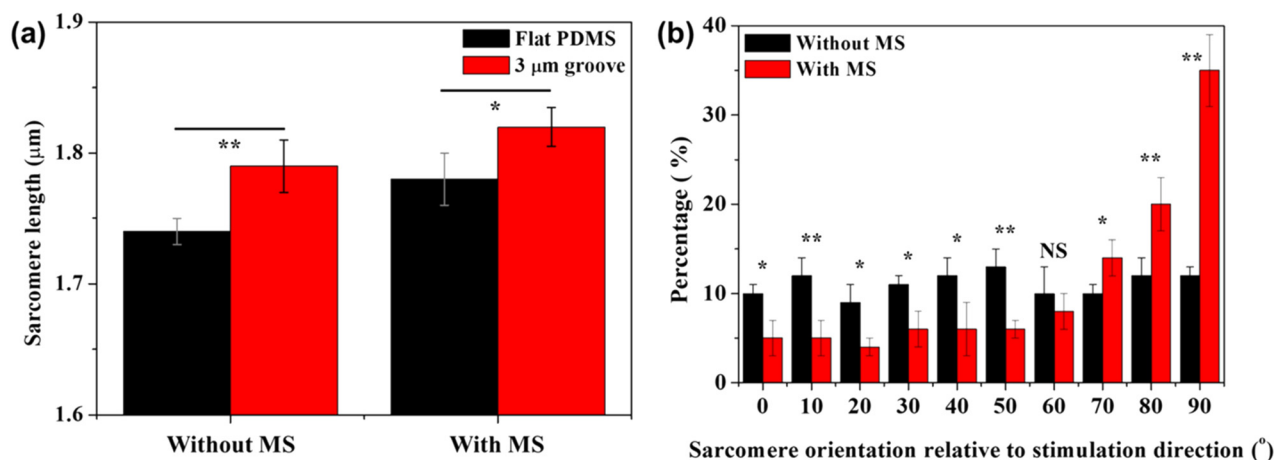


Fig. 3 Effect of both topographical and mechanical stimulation on cultured cardiomyocytes on flat and microgrooved PDMS membranes with and without mechanical stimulation under 10% applied tensile stress at a frequency of 1 Hz. (a) Sarcomere length of cardiomyocytes cultured on both types of PDMS membranes with and without mechanical stimulation. (b) Analysis of sarcomere length in cardiomyocytes obtained from different regions of the PDMS diaphragm under mechanical stimulation. The bars and error bars indicate the mean \pm standard deviation ($n = 6$). NS (non-significant), * $P < 0.05$, ** $P < 0.01$.

direction of cardiomyocytes cultured on the grooved PDMS membrane with and without mechanical stimulation was assessed, as shown in Fig. 3b. Cardiomyocytes cultured perpendicular to the direction of mechanical stimulation were subjected to the highest intensity of mechanical stimulation, resulting in a significant increment in sarcomere length as the angle progressed from 0° to 90°. Only 35% of the cardiomyocytes' sarcomeres aligned vertically and exhibited growth in response to mechanical stimulation, while in the absence of mechanical stimulation, the cells proliferated without any specific orientation.

Subsequently, the synergistic effect of a conductive cell culture substrate in conjunction with topographical and mechanical stimulation on cardiomyocyte proliferation and maturation was investigated, as shown in Fig. 4. Cardiomyocytes were cultured on grooved PDMS, AgNWs-S-PDMS, and AgNWs-E-PDMS membranes and exposed to mechanical stimulation at 10% tensile stress with a frequency of 1 Hz from culture days 4 to 10. After the cultivation period,

the cardiomyocytes were collected from the central region of the cell culture substrate and subjected to ICC staining analysis (Fig. 4a). Cardiomyocytes cultured on all PDMS membranes aligned in the groove direction due to the topographical stimulation. However, those subjected to mechanical stimulation and cultured on AgNWs-E-PDMS exhibited a more organized structure compared to those cultured on bare grooved PDMS and AgNWs-S-PDMS membranes.

The cardiomyocytes cultured on grooved PDMS membranes exhibited an average sarcomere length of $1.81 \pm 0.005 \mu\text{m}$. In contrast, cardiomyocytes cultured on the AgNWs-S-PDMS and AgNWs-E-PDMS membranes displayed slightly longer sarcomere lengths of $1.82 \pm 0.009 \mu\text{m}$ and $1.82 \pm 0.01 \mu\text{m}$, respectively. Under mechanical stimulation, the cardiomyocytes cultured on grooved PDMS, AgNWs-S-PDMS, and AgNWs-E-PDMS membranes demonstrated sarcomere lengths of $1.84 \pm 0.007 \mu\text{m}$, $1.85 \pm 0.01 \mu\text{m}$, and $1.86 \pm 0.01 \mu\text{m}$, respectively. The highest sarcomere length was observed in cardiomyocytes cultured on AgNWs-E-PDMS membranes

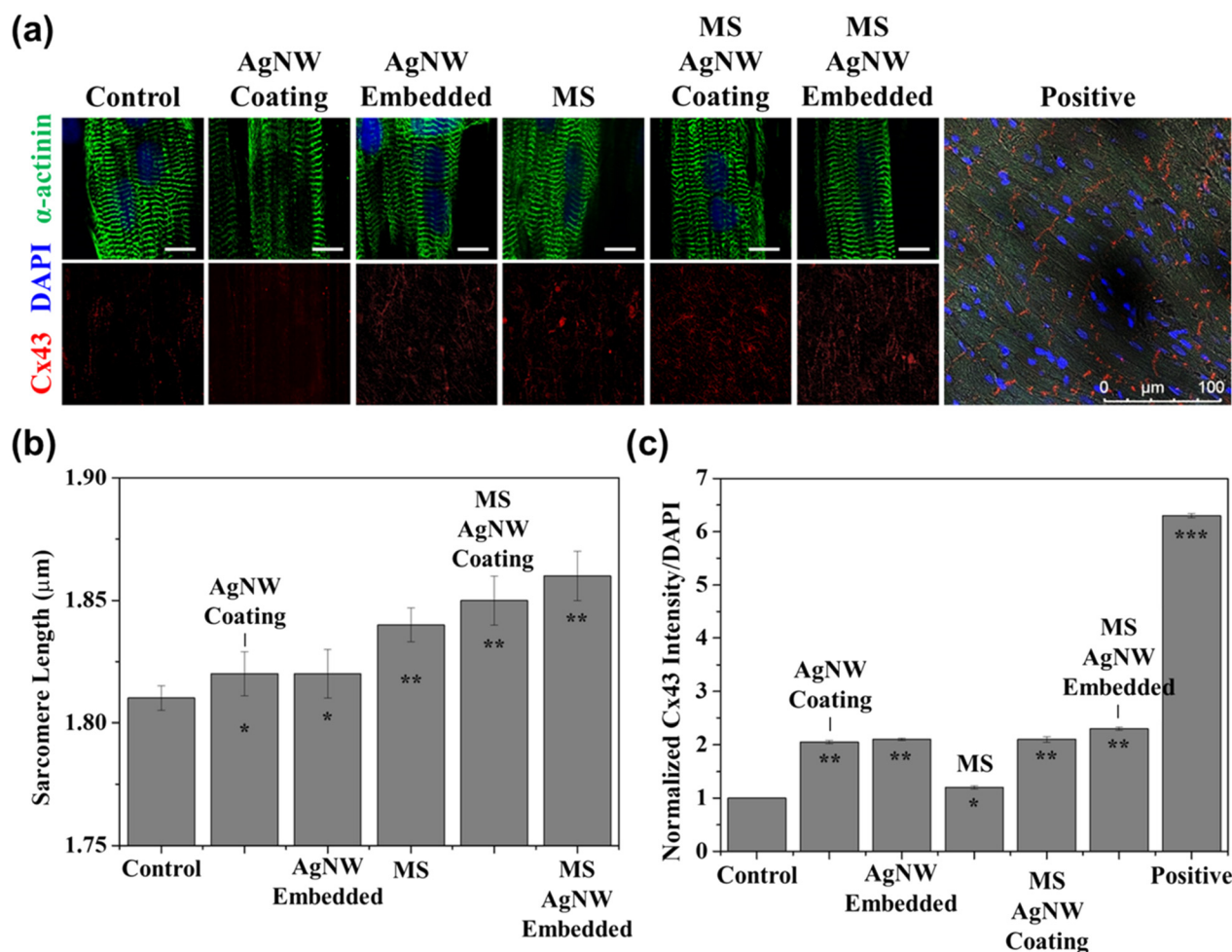


Fig. 4 Synergistic effect of conductive substrates with topographical stimulation and mechanical stimulation on cardiomyocyte growth and maturation. (a) Immunocytochemical staining of cardiomyocytes cultured on bare grooved PDMS, AgNWs-S-PDMS, and AgNWs-E-PDMS, subjected to mechanical stimulation at 10% tensile stress and 1 Hz frequency for 7 days. (b and c) Sarcomere length and Cx43 expression in cardiomyocytes cultured on bare grooved PDMS, AgNWs-S-PDMS, and AgNWs-E-PDMS, with mechanical stimulation at 10% tensile stress and 1 Hz frequency for 7 days. Bars and error bars represent mean \pm standard deviation ($n = 6$). * $P < 0.05$, ** $P < 0.01$, *** $P < 0.001$.

coupled with mechanical stimulation, which indicates an enhanced degree of maturation (Fig. 4b).

The expression levels of Cx43, a protein integral to cardiac function, were evaluated in cardiomyocytes cultured on bare grooved PDMS, AgNWs-S-PDMS, and AgNWs-E-PDMS membranes, in the presence of mechanical stimulation (Fig. 4c). Compared to the control group, cardiomyocytes cultured on AgNWs-S-PDMS and AgNWs-E-PDMS membranes displayed a 2-fold enhancement in Cx43 expression, indicating an effective response to the conductive substrate. Moreover, when the cardiomyocytes were subjected to mechanical stimulation, a further amplification of Cx43 expression was observed, resulting in increases of 2.2 and 2.4 times relative to the controls. The ICC staining analysis demonstrated that the interaction of mechanical stimulation with the embedded AgNWs led to a more than two-fold enhancement in Cx43 expression within one-week NRVM targets. This upregulation in Cx43 protein expression subsequently led to an increase in gap junction formation and growth protein expression in the cardiomyocytes, thereby enhancing their contractile properties. While the degree of Cx43 expression increase was less pronounced compared to that of a 17 week-old mature adult rat (used as a positive control), the observed growth within a short period illustrates a significant trend towards maturation, highlighting the potential of both mechanical stimulation and conductive AgNWs in promoting cardiomyocyte maturation.

The contractile properties of cardiomyocytes cultured on both bare grooved PDMS and AgNWs-E-PDMS membranes were investigated through video tracking analysis (Fig. 5). Optical micrographs demonstrated the alignment of the cardiomyocytes cultured on both bare PDMS and AgNWs-E-PDMS membranes in the groove direction. The arrows in the optical micrographs indicate two specific cardiomyocytes selected for detailed contractility analysis (Fig. 5a). The contractility of the cardiomyocytes was measured by capturing video footage with a confocal microscope and subsequently analysing the movement of cardiomyocytes using tracking software. The corresponding contractile behaviours of cardiomyocytes, cultured on both bare grooved PDMS and AgNWs-E-PDMS membranes at locations a and b, are shown in Fig. 5b. The cardiomyocytes cultured on bare grooved PDMS membranes displayed asynchronous contraction and relaxation, while the contractility of the cardiomyocytes cultured on AgNWs-E-PDMS membranes exhibited harmonious synchronization across different regions. Moreover, an increase in contraction force by 0.5 μm was observed in cardiomyocytes cultured on AgNWs-E-PDMS membranes in comparison to those cultured on bare grooved PDMS membranes. Time-delay mapping demonstrated the superior degree of synchronized beating in cardiomyocytes grown on AgNWs-E-PDMS membranes compared to those cultured on bare grooved PDMS membranes (Fig. 5c). This synchronization is indicative of improved cell-cell communication and coordinated contractile behaviour, which are crucial factors for proper cardiac tissue function and maturation. Enhanced synchronization on the AgNWs-E-PDMS membranes could be attributed to the combined effects of the conductive substrate and topographical cues, promoting the formation of a more organized and mature cardiomyocyte network.

The contraction properties of cardiomyocytes cultured on bare grooved PDMS and AgNWs-E-PDMS membranes, in both the absence and presence of mechanical stimulation, were quantitatively evaluated, as shown in Fig. 6. The real-time contraction kinetics of cardiomyocytes cultured under different conditions such as the grooved PDMS membrane and AgNWs-E-PDMS membrane, both with and without mechanical stimulation, are shown in Fig. 6a-d. The corresponding bar diagram demonstrates the normalized contraction forces of the cardiomyocytes cultured under the four distinct conditions – bare grooved PDMS and AgNWs-E-PDMS, and bare grooved PDMS and AgNWs-E-PDMS membrane with applied mechanical stimulation. The contractility of the cardiomyocytes cultured under the four different experimental conditions was found to be 1.0 ± 0.1 , 1.5 ± 0.15 , 1.8 ± 0.1 , and 2.0 ± 0.15 μm , respectively. Remarkably, cardiomyocytes exhibited a two-fold enhancement in contraction force when cultured on the AgNWs-E-PDMS membrane with mechanical stimulation, in comparison to those grown on the bare grooved PDMS membrane.

The contractility of cardiomyocytes cultured on AgNWs-S-PDMS and AgNWs-E-PDMS membranes was investigated over

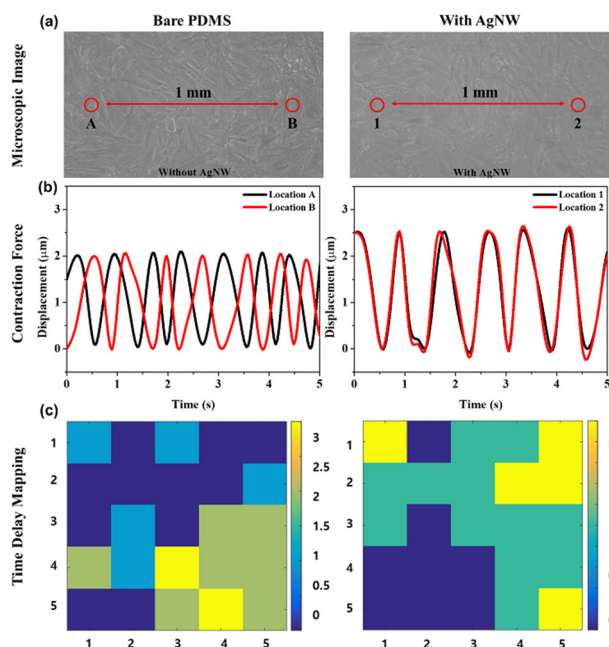


Fig. 5 Contractile properties of cardiomyocytes cultured on bare grooved PDMS and AgNWs-E-PDMS membranes. (a and b) Optical micrographs and corresponding contraction force measurements for cardiomyocytes cultured on bare PDMS and AgNWs-E-PDMS membranes. (c) Time-delay mapping illustrating the synchronization of cardiomyocytes cultured on bare grooved PDMS and AgNWs-E-PDMS membranes.

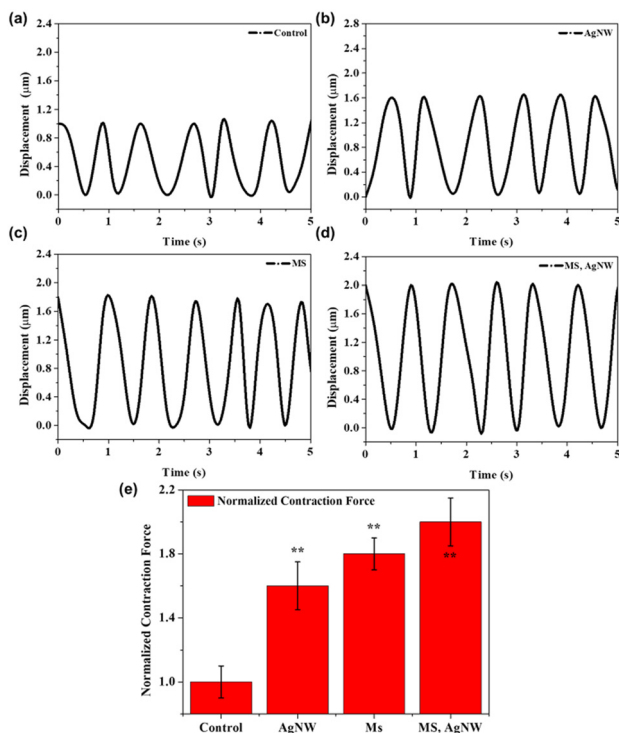


Fig. 6 Contractile properties of cardiomyocytes cultured on bare grooved PDMS membrane, AgNWs-E-PDMS membrane, and bare grooved PDMS with mechanical stimulation at 10% tensile stress and 1 Hz frequency. (a–d) Real-time traces of cardiomyocyte contractility in response to varying cell culture substrate properties and mechanical stimulation. (e) Bar plot displaying the normalized contraction force of cardiomyocytes based on cell culture substrate characteristics and mechanical stimulation. Bars and error bars represent the mean \pm standard deviation ($n = 6$). * $P < 0.05$, ** $P < 0.01$.

a culture period ranging from day 3 to day 24. Real-time traces of cardiomyocyte contractility on these membranes are shown in Fig. S11a and b.† The normalized contraction force of the cultured cardiomyocytes on both types of membranes exhibited an increasing trend until day 12, after which it gradually declined. This pattern suggests that a subset of cardiomyocytes began to detach and aggregate as the incubation period increased. The relative contraction force and beat rate of these cultured cardiomyocytes are shown Fig. S11c and d.† Cardiomyocytes cultured on the AgNWs-E-PDMS membrane demonstrated significantly enhanced normalized contraction forces compared to those on the AgNWs-S-PDMS membrane. Additionally, cardiomyocytes on the AgNWs-S-PDMS membrane survived for only up to 15 days before detaching due to cellular senescence, whereas those on the AgNWs-E-PDMS membrane survived until day 24 and produced a measurable contraction force. These outcomes suggest that the AgNWs-E-PDMS membrane facilitates superior cell adhesion, cell-cell interactions, and cardiomyocyte maturation, as evidenced by a longer lifespan, greater contraction force, and stable beat rate, compared to the AgNWs-S-PDMS membrane. The practical feasibility of the proposed device as a drug screening platform was

demonstrated by quantifying the drug-induced adverse effects on cardiomyocytes that were cultured under four different conditions, such as the bare-groove PDMS membrane, AgNWs-E-PDMS membrane, and bare-groove PDMS membrane with mechanical stimulation, and AgNWs-E-PDMS membrane with mechanical stimulation. The drug dose response analysis of the cardiomyocytes was carried out following a cultivation period of nine days, during which the cardiomyocytes exhibited stable contractile behaviour. Lidocaine, a prototypical cardiovascular agent, was employed to investigate its adverse effects on cultured cardiomyocytes. As a sodium ion channel blocker, lidocaine exerts a significant effect on the cardiomyocyte contractility and beat rate. Lidocaine has been widely used as an antiarrhythmic drug for controlling ventricular arrhythmias. In rare instances, inadequate administration of lidocaine may lead to severe complications, such as allergic reactions or systemic toxicity. The desired concentration (IC_{50} 22 μ M) of lidocaine was prepared by diluting the drug in ethanol. Subsequently, the cardiomyocytes were exposed to 22 μ M of lidocaine for investigating its adverse effects on the contractility of the

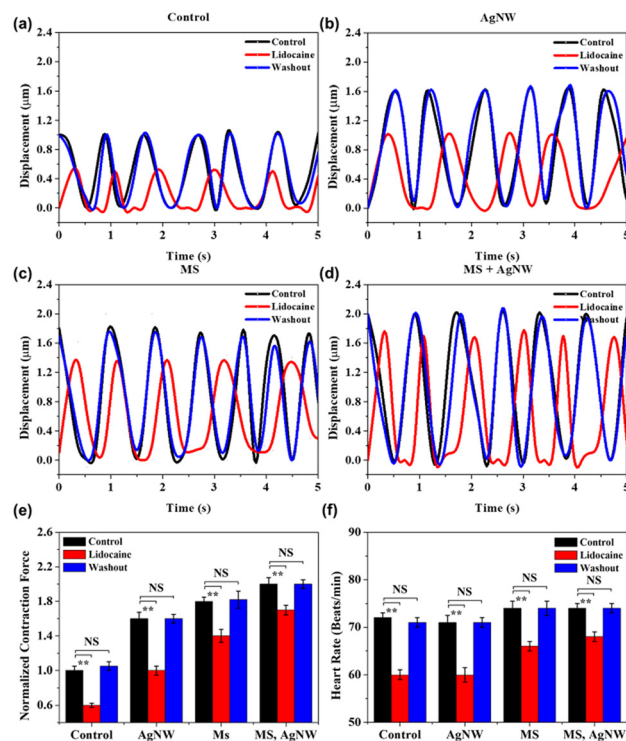


Fig. 7 Effect of drug induced changes on cardiomyocyte contractile properties in relation to the cell culture substrate and mechanical stimulation. (a–d) Real-time traces of cardiomyocytes cultured on bare-groove PDMS membranes, AgNWs-E-PDMS, bare-groove PDMS membranes with mechanical stimulation, and AgNWs-E-PDMS membranes with mechanical stimulation prior to and following lidocaine treatment, as well as after a 24 h drug washout period. (e and f) Bar graphs represent the normalized contraction force and beat frequency of cardiomyocytes as a function of cell culture substrate and mechanical stimulation before and after lidocaine exposure, and post-24 h drug washout. The bars and error bars indicate the mean \pm standard deviation ($n = 6$). NS (non-significant), * $P < 0.05$, ** $P < 0.01$.

cardiomyocytes. The contractile characteristics of the cardiomyocytes were assessed prior to and following the treatment with 22 μM lidocaine and after 24 h following the replacement with fresh culture medium. Fig. 7a–d shows the real-time traces of cardiomyocyte contraction force before and after lidocaine treatment, as well as after a 24 h period of drug washout. Lidocaine decreased both the contractility and beat rate of cardiomyocytes cultured under all four different conditions. The bar plot shows the normalized contraction force of cardiomyocytes before and after drug treatment, as well as after a 24 h period of fresh culture medium replacement (Fig. 7e). Prior to drug treatment, the normalized contraction force of the cardiomyocytes was found to be 1.0 ± 0.1 , 1.5 ± 0.15 , 1.8 ± 0.1 , and 2.0 ± 0.15 for bare-groove PDMS, AgNWs-E-PDMS, bare-groove PDMS membrane with mechanical stimulation, and AgNWs-E-PDMS membrane with mechanical stimulation, respectively. Following the treatment with 22 μM lidocaine, the contraction forces of cardiomyocytes cultured on bare-groove PDMS, AgNWs-E-PDMS, bare-groove PDMS membrane with mechanical stimulation, and AgNWs-E-PDMS membrane with mechanical stimulation were decreased to 0.6, 0.73, 0.77, and 0.9 times their respective initial values. The beat rates of cardiomyocytes cultured on bare-groove PDMS membrane, AgNWs-E-PDMS membrane, bare-groove PDMS membrane with mechanical stimulation, and AgNWs-E-PDMS membrane with mechanical stimulation before treatment were about 78 ± 2 and, upon treatment with 22 μM lidocaine, decreased to 0.51, 0.58, 0.61, and 0.64 times the respective control state (Fig. 7f). Furthermore, cardiomyocytes cultured on all cell culture substrates retained their intrinsic contraction force levels and beat rates 24 h after drug washout. The relatively smaller changes in contraction force and beat rate observed in cardiomyocytes cultured on the AgNWs-E-PDMS membrane with mechanical stimulation indicate an enhanced drug response due to improved maturation and growth of the cells.

Secondly, the effect of verapamil on the cardiomyocytes cultured on the proposed bare groove PDMS and AgNWs-E-PDMS drug screening platforms was investigated. Verapamil is widely used to treat hypertension, angina, and certain types of arrhythmias. It is a class IV antiarrhythmic drug and an L-type calcium channel blocker that inhibits the inflow of calcium ions into cardiomyocytes, resulting in a decrease in cardiomyocyte contractility. Therefore, it is necessary to investigate the adverse effects of verapamil on the cultured cardiomyocytes. The contractility of the cultured cardiomyocytes was investigated before and after treating the cardiomyocytes with 133 nM verapamil and after 24 h following the replacement of fresh culture medium, as shown in Fig. 8. As expected, the quantitative analyses revealed a decline in both contractile characteristics and beat rate in cardiomyocytes cultivated on various substrates and conditions: bare-groove PDMS membranes, AgNWs-E-PDMS membranes, and their mechanically stimulated counterparts (Fig. 8a–d).

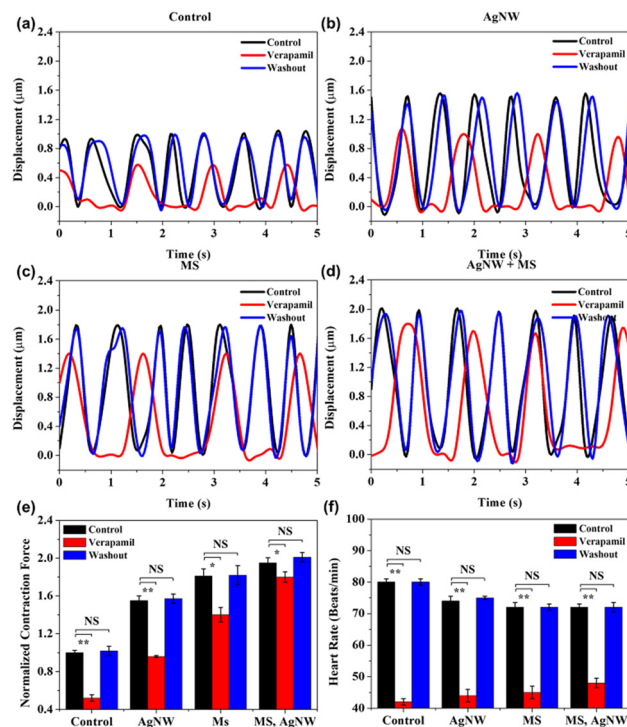


Fig. 8 Effect of drug induced changes on cardiomyocyte contractile properties in relation to the cell culture substrate and mechanical stimulation. (a–d) Real-time traces of cardiomyocytes cultured on bare-groove PDMS membranes, AgNWs-E-PDMS, bare-groove PDMS membranes with mechanical stimulation, and AgNWs-E-PDMS membranes with mechanical stimulation prior to and following verapamil treatment, as well as after a 24 h drug washout period. (e and f) Bar graphs represent the normalized contraction force and beat frequency of cardiomyocytes as a function of cell culture substrate and mechanical stimulation before and after lidocaine exposure, and post-24 h drug washout. The bars and error bars indicate the mean \pm standard deviation ($n = 6$). NS (non-significant), * $P < 0.05$, ** $P < 0.01$.

The bar graph in Fig. 8e shows the normalized contraction forces of these cardiomyocytes pre- and post-administration of 133 nM verapamil, as well as after a 24 h period of fresh culture medium replenishment. Prior to verapamil treatment, the measured normalized contraction forces for cardiomyocytes on bare-groove PDMS, AgNWs-E-PDMS, mechanically stimulated bare-groove PDMS, and mechanically stimulated AgNWs-E-PDMS were 1.00 ± 0.05 , 1.55 ± 0.10 , 1.81 ± 0.15 , and 1.95 ± 0.11 , respectively. After verapamil treatment, these values were decreased to 0.52 ± 0.07 , 0.96 ± 0.02 , 1.42 ± 0.15 , and 1.8 ± 0.11 , respectively. Fig. 8f shows that the beat rates of the cardiomyocytes cultured on the bare-groove PDMS and AgNWs-E-PDMS membranes were 80 ± 2 and 74 ± 3 , respectively, which, after verapamil treatment, were reduced to 52% and 66% of their respective control states. Importantly, all cardiomyocytes exhibited recovery of their intrinsic contractile function and beat frequencies 24 h subsequent to drug washout.

We also encompassed an evaluation of the cardiomyocyte response to isoproterenol, a known β -1 adrenergic receptor drug that causes a dose-dependent positive inotropic effect on

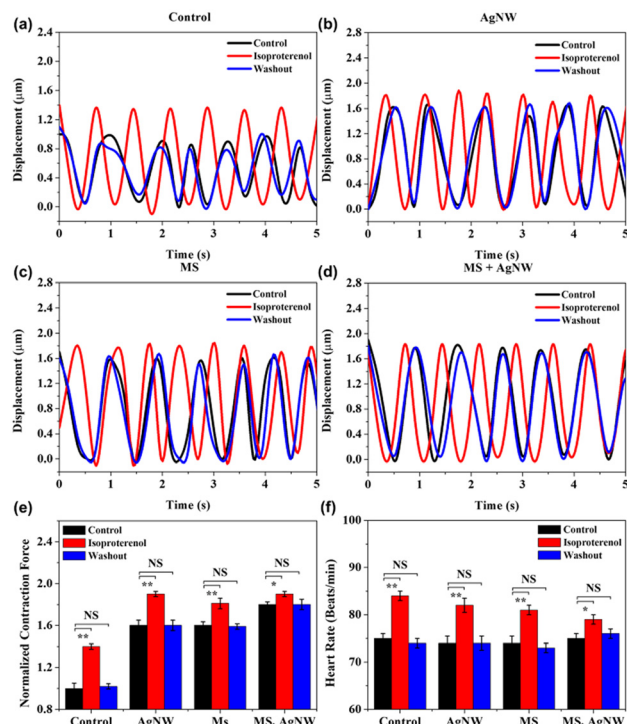


Fig. 9 Effect of drug induced changes on cardiomyocyte contractile properties in relation to the cell culture substrate and mechanical stimulation. (a–d) Real-time traces of cardiomyocytes cultured on bare-groove PDMS membranes, AgNWs–E-PDMS, bare-groove PDMS membranes with mechanical stimulation, and AgNWs–E-PDMS membranes with mechanical stimulation prior to and following isoproterenol treatment, as well as after a 24 h drug washout period. (e and f) Bar graphs represent the normalized contraction force and beat frequency of cardiomyocytes as a function of cell culture substrate and mechanical stimulation before and after lidocaine exposure, and post-24 h drug washout. The bars and error bars indicate the mean \pm standard deviation ($n = 6$). NS (non-significant), * $P < 0.05$, ** $P < 0.01$.

cardiomyocytes, thereby increasing their contractile force. Cardiomyocytes cultivated on both bare-grooved PDMS and AgNWs–E-PDMS membranes were exposed to a 10 μ M concentration of isoproterenol. Real-time traces describing the dynamic changes in cardiomyocyte contractility on these substrates—both in the absence and presence of mechanical stimulation—pre- and post-isoproterenol treatment are shown in Fig. 9a–d. The bar graphs in Fig. 9e and f provide a quantitative analysis of the normalized contraction force and beat rate for cardiomyocytes under these varied experimental conditions. In the absence of mechanical stimulation, the normalized contraction forces were quantified as 1.00 ± 0.10 and 1.61 ± 0.11 for the bare-grooved PDMS and AgNWs–E-PDMS membranes, respectively. In the presence of mechanical stimulation, the contraction force of the cardiomyocytes significantly increased to 1.61 ± 0.08 for bare-grooved PDMS and 1.82 ± 0.05 for AgNWs–E-PDMS. Comparative analysis revealed that upon treatment with 10 μ M isoproterenol, the normalized contraction force of the cardiomyocytes cultured on both substrates—both with and without mechanical stimulation—increased by respective factors of 1.82, 1.77, 1.53, and 1.13.

The beat rates for cardiomyocytes under the four experimental conditions—bare-grooved PDMS, AgNWs–E-PDMS, mechanically stimulated bare-grooved PDMS, and mechanically stimulated AgNWs–E-PDMS—were found to be 75 ± 2 , 74 ± 3 , 74 ± 3 , and 75 ± 2 , respectively. Following isoproterenol administration, these beat rates exhibited increments, registering at 84 ± 2 , 82 ± 3 , 81 ± 2 , and 79 ± 2 , respectively.

Conclusion

In conclusion, we have developed a drug screening platform for investigating drug-induced cardiotoxicity. The mechanical stimulation system developed in this study consists of a step motor, linear stage, laser vibrometer, functional well plate, and stage-top incubator. Cardiomyocytes derived from NRVMs were cultured on a cell culture substrate. We systematically conducted a comprehensive investigation into the maturation of cardiomyocytes, considering the effects of topographical and mechanical stimulation, as well as the use of a conductive cell culture substrate. The proliferation and maturation of cardiomyocytes were assessed through ICC staining analysis. The results demonstrated that cardiomyocytes subjected to 10% tensile stress on the AgNWs–E-PDMS membrane exhibited significant improvements in sarcomere length and Cx43 expression compared to the control group. Furthermore, we investigated the adverse effects of a typical cardiovascular drug, lidocaine, on cardiomyocytes cultured on the proposed device. Cardiomyocytes exposed to mechanical stimulation on the AgNWs–E-PDMS membrane displayed more pronounced drug responses compared to cells cultured without mechanical stimulation or a conductive substrate. Overall, our proposed drug screening platform holds great potential for application in various fields of cell biology and regenerative medicine.

Author contributions

Jongyun Kim: conceptualisation; investigation; formal analysis; data curation; visualisation; writing – original draft. Arunkumar Shanmugasundaram: investigation; writing – original draft; review and editing. Cheong Bin Lee: formal analysis; data curation. Jae Rim Kim: formal analysis; data curation. Jeong Jae Park: formal analysis; data curation. Eung-Sam Kim: formal analysis; data curation, reviewing and editing. Bong-Kee Lee: formal analysis; data curation, reviewing and editing. Dong-Weon Lee: supervised the project; funding acquisition; supervision; conceptualisation; methodology; software; validation; formal analysis; data curation; visualisation; writing – original draft, reviewing, and editing.

Conflicts of interest

No conflicts of interest to declare.

Acknowledgements

This work was supported by the National Research Foundation of Korea (NRF) grant funded by the Korean government (MSIT) (No. 2020R1A5A8018367 & 2022R1A6A3A01087316).

Notes and references

- 1 S. C. Smith, A. Collins, R. Ferrari, D. R. Holmes, S. Logstrup, D. V. McGhie, J. Ralston, R. L. Sacco, H. Stam, K. Taubert, D. A. Wood and W. A. Zoghbi, *Circulation*, 2012, **126**, 2769–2775.
- 2 P. Bhatnagar, K. Wickramasinghe, J. Williams, M. Rayner and N. Townsend, *Heart*, 2015, **101**, 1182–1189.
- 3 R. Mehra, *J. Electrocardiol.*, 2007, **40**, s118–s122.
- 4 H. Savoji, M. H. Mohammadi, N. Rafatian, M. K. Toroghi, E. Y. Wang, Y. Zhao, A. Korolj, S. Ahadian and M. Radisic, *Biomaterials*, 2019, **198**, 3–26.
- 5 C. G. Tocchetti, *et al.*, *Antioxid. Redox Signaling*, 2019, **30**, 2110–2153.
- 6 V. Tabar and L. Studer, *Nat. Rev. Genet.*, 2014, **15**, 82–92.
- 7 G.-S. Cho, L. Fernandez and C. Kwon, *Antioxid. Redox Signaling*, 2014, **21**, 2018–2031.
- 8 R. R. Besser, M. Ishahak, V. Mayo, D. Carbonero, I. Claure and A. Agarwal, *Theranostics*, 2018, **8**, 124–140.
- 9 N. T. Feric and M. Radisic, *Adv. Drug Delivery Rev.*, 2016, **96**, 110–134.
- 10 I. Nitsan, S. Drori, Y. E. Lewis, S. Cohen and S. Tzlil, *Nat. Phys.*, 2016, **12**, 472–477.
- 11 M. Lux, B. Andrée, T. Horvath, A. Nosko, D. Manikowski, D. Hilfiker-Kleiner, A. Haverich and A. Hilfiker, *Acta Biomater.*, 2016, **30**, 177–187.
- 12 J. Zhuang, K. A. Yamada, J. E. Saffitz and A. G. Kléber, *Circ. Res.*, 2000, **87**, 316–322.
- 13 V. Y. Sidorov, P. C. Samson, T. N. Sidorova, J. M. Davidson, C. C. Lim and J. P. Wikswo, *Acta Biomater.*, 2017, **15**, 68–78.
- 14 M. Shachar, N. Benishti and S. Cohen, *Biotechnol. Prog.*, 2012, **28**, 6.
- 15 A. Marsano, C. Conficconi, M. Lemme, P. Occhetta, E. Gaudiello, E. Votta, G. Cerino, A. Redaelli and M. Rasponi, *Lab Chip*, 2016, **16**, 599.
- 16 Y. Kamotani, T. Bersano-Begey, N. Kato, Y.-C. Tung, D. Huh, J. W. Song and S. Takayama, *Biomaterials*, 2008, **29**, 2646–2655.
- 17 X. Tang, P. Bajaj, R. Bashir and T. A. Saif, *Soft Matter*, 2011, **7**, 6151.
- 18 W. Dou, L. Wang, M. Malhi, H. Liu, Q. Zhao, J. Plakhotnik, Z. Xu, Z. Huang, C. A. Simmons, J. T. Maynes and Y. Sun, *Biosens. Bioelectron.*, 2021, **175**, 112875.
- 19 Y.-J. Jeong, D.-S. Kim, J. Y. Kim, N.-E. OYunbaatar, A. Shanmugasundaram, E.-S. Kim and D.-W. Lee, *Mater. Sci. Eng., C*, 2021, **118**, 111355.
- 20 A.-B. Siddique, A. Shanmugasundaram, J. Y. Kim, A. Roshanzadeh, E.-S. Kim, B.-K. Lee and D.-W. Lee, *Biosens. Bioelectron.*, 2022, **204**, 114017.
- 21 I. J. Gómez, M. V. Sulleiro, D. Mantione and N. Alegret, *Polymers*, 2021, **13**, 745.
- 22 G. Kaur, R. Adhikari, P. Cass, M. Bown and P. Gunatillake, *RSC Adv.*, 2015, **5**, 37553.
- 23 H. He, L. Zhang, X. Guan, H. Cheng, X. Liu, S. Yu, J. Wei and J. Ouyang, *ACS Appl. Mater. Interfaces*, 2019, **11**, 26185–26193.
- 24 L. Yang, Y. Wu, F. Yang and W. Wang, *RSC Adv.*, 2021, **11**, 20081.
- 25 A. S. T. Smith, H. Yoo, H. Yi, E.-H. Ahn, J. Lee, G. Shao, E. Nagornyak, M. A. Laflamme, C. E. Murry and D.-H. Kim, *Chem. Commun.*, 2017, **53**, 7412–7415.
- 26 J. Kim, A. Shanmugasundaram and D.-W. Lee, *Analyst*, 2021, **146**, 6768–6779.
- 27 L. Hu, H. S. Kim, J.-Y. Lee, P. Peumans and Y. Cui, *ACS Nano*, 2010, **4**, 2955–2963.
- 28 M. A. Shinde, K. Mallikarjuna, J. Noh and H. Kim, *Thin Solid Films*, 2018, **660**, 447–454.
- 29 R. Cheng, J. Zeng, B. Wang, J. Li, Z. Cheng, J. Xu, W. Gao and K. Chen, *Chem. Eng. J.*, 2021, **424**, 130565.
- 30 S. M. Jeong, J.-H. Kim, S. Song, J. Seo, J.-I. Hong, N. Y. Ha, H. Takezoe, J. Jeong and H. Kim, *RSC Adv.*, 2015, **5**, 51086.
- 31 Y. Li, P. Cui, L. Wang, H. Lee, K. Lee and H. Lee, *ACS Appl. Mater. Interfaces*, 2013, **5**, 9155–9160.
- 32 S.-W. Yeom, B. You, K. Cho, H. Y. Jung, J. Park, C. Shin, B.-K. Ju and J.-W. Kim, *Sci. Rep.*, 2017, **7**, 3438.
- 33 H. J. Yun, S. J. Kim, J. H. Hwang, Y. S. Shim, S.-G. Jung, Y. W. Park and B.-K. Ju, *Sci. Rep.*, 2016, **6**, 34150.
- 34 K. Kim, J. Kim, B. G. Hyun, S. Ji, S.-Y. Kim, S. Kim, B. W. An and J.-U. Park, *Nanoscale*, 2015, **7**, 14577.
- 35 Y. Han, R. Lupitsky, T.-M. Chou, C. M. Stafford, H. Du and S. Sukhishvili, *Anal. Chem.*, 2011, **83**, 5873–5880.
- 36 W. H. Chae, T. Sanniccolo and J. C. Grossman, *ACS Appl. Mater. Interfaces*, 2020, **12**, 17909–17920.
- 37 B.-Y. Wang, E.-S. Lee, Y.-J. Oh and H. W. Kang, *RSC Adv.*, 2017, **7**, 52914.
- 38 A. Wickham, M. Vagin, H. Khalaf, S. Bertazzo, P. Hodder, S. Danmark, T. Bengtsson, J. Altimiras and D. Aili, *Nanoscale*, 2016, **8**, 14146.
- 39 S. Jiang and C. P. Teng, *Mater. Sci. Eng., C*, 2017, **70**, 1011–1017.
- 40 Y. Liu, N.-E. OYunbaatar, A. Shanmugasundaram, E.-S. Kim, B.-K. Lee and D.-W. Lee, *Sens. Actuators, B*, 2023, **390**, 134014.
- 41 J. Y. Kim, Y.-S. Choi, B.-K. Lee and D.-W. Lee, *Biosens. Bioelectron.*, 2016, **80**, 456–462.